

# Geophysical Research Letters®



## RESEARCH LETTER

10.1029/2022GL101693

### Key Points:

- The magnetic field structures at magnetotail jet fronts (JFs) are statistically investigated using a database of 2394 bursty bulk flows
- Solitary dipolarization fronts (DFs) are found at only 10% of the JFs
- DFs with more complex structures are more common and are found at 32% of the JFs

### Correspondence to:

L. Richard,  
[louis.richard@irfu.se](mailto:louis.richard@irfu.se)

### Citation:

Richard, L., Khotyaintsev, Y. V., Graham, D. B., & Russell, C. T. (2022). Are dipolarization fronts a typical feature of magnetotail plasma jets fronts? *Geophysical Research Letters*, 49, e2022GL101693. <https://doi.org/10.1029/2022GL101693>

Received 31 OCT 2022  
Accepted 10 NOV 2022

## Are Dipolarization Fronts a Typical Feature of Magnetotail Plasma Jets Fronts?

L. Richard<sup>1,2</sup> , Yu. V. Khotyaintsev<sup>1</sup> , D. B. Graham<sup>1</sup> , and C. T. Russell<sup>3</sup> 

<sup>1</sup>Swedish Institute of Space Physics, Uppsala, Sweden, <sup>2</sup>Space and Plasma Physics, Department of Physics and Astronomy, Uppsala University, Uppsala, Sweden, <sup>3</sup>Department of Earth Planetary and Space Sciences, University of California Los Angeles, Los Angeles, CA, USA

**Abstract** Plasma jets are ubiquitous in the Earth's magnetotail. Plasma jet fronts (JFs) are a seat of particle acceleration and energy conversion. JFs are commonly associated with dipolarization fronts (DFs), which are often characterized by solitary sharp large-amplitude increases in the northward component of the magnetic field  $B_z$ . However, MHD and kinetic instabilities can develop at JFs and disturb the front structure which questions on the occurrence of solitary DFs at the JFs. We investigate the structure of JFs using 5 years (2017–2021) of the Magnetospheric Multiscale observations in the central plasma sheet (CPS) in the Earth's magnetotail. We compiled a database of 2394 CPS jets. We find that 42% of the JFs are associated with large-amplitude changes in  $B_z$ . However, solitary DFs constitute a quarter of these large-amplitude events, while the rest are associated with more complex structures.

**Plain Language Summary** We statistically investigate the magnetic field structure associated with the leading edge of fast plasma flows (jets), in the nightside region of the Earth's magnetosphere. Owing to its stretched magnetic field configuration, this region is called the magnetotail. The magnetotail plasma jets transport magnetic flux in the form of structures carrying an intense dipole-like magnetic field. It is commonly assumed that the leading edge of the structures convected by the plasma jet is a sharp change of the magnetic field configuration from a stretched to dipole-like configuration called a dipolarization front (DF). However, the plasma jet provides a source of free energy that dissipates through various instabilities which grow at the leading edge of the plasma jet. Hence, we suspect that the sharp vertical boundary is often strongly perturbed. Using the Magnetospheric Multiscale spacecraft observations, we find that the solitary DFs are seen in only 10% of the plasma jet fronts (JFs). On the other hand, we found that 32% of the plasma JFs are associated with magnetic field structures, which are more complex than solitary DFs. Our result questions the commonly accepted picture of DFs as the leading edge of magnetotail plasma jets.

## 1. Introduction

Magnetotail bursty bulk flows (BBFs) (Baumjohann et al., 1990) are transient (10–100 s) fast plasma jets in the central plasma sheet (CPS). Earthward BBFs are responsible for the majority of the plasma and magnetic flux transport from the magnetotail to the inner magnetosphere (Angelopoulos et al., 1994). The jet fronts (JFs) are often accompanied by a sharp ion-scale magnetic field structures called dipolarization fronts (DFs) (Nakamura et al., 2002; Ohtani et al., 2004; Runov et al., 2011). DFs are identified in spacecraft data as solitary sharp large-amplitude increases in the northward component of the magnetic field  $B_z$  (Fu et al., 2012; Runov et al., 2011). Upstream of the DF, the magnetic field configuration is that of the unperturbed CPS with a small  $B_z$  normal to the magnetotail current sheet. DFs are often preceded by a depletion of  $B_z$  before the sharp increase of  $B_z$  at the front (Runov et al., 2009; Schmid et al., 2011). Following the front  $B_z$  slowly 20 s decreases to its initial upstream value (Runov et al., 2011). DFs are ion-inertial-length-scale (Schmid et al., 2011) boundaries separating low temperature dense plasma in the preexisting CPS from hotter tenuous plasma (Khotyaintsev et al., 2011; Runov et al., 2011). In the cross-tail dawn-dusk direction DFs extend over  $\sim 1\text{--}5 R_E$  (Liu et al., 2015; Sergeev et al., 1996). DFs are thought to be a result of transient unsteady magnetic reconnection (Sitnov et al., 2009) or detachment of interchange heads in the nonlinear stage of the kinetic ballooning interchange instability (Pritchett & Coroniti, 2010). Because of their distinct signature, DFs and their contribution to the magnetotail energy budget have been extensively investigated using case studies (Angelopoulos et al., 2013; Artemyev et al., 2012; Fu et al., 2011; Khotyaintsev et al., 2017) and statistical studies (Fu et al., 2012; Runov et al., 2011; Schmid et al., 2011, 2019). These studies focused on DFs, and thus omitted other JFs with more complicated magnetic

© 2022. The Authors.

This is an open access article under the terms of the [Creative Commons Attribution License](https://creativecommons.org/licenses/by/4.0/), which permits use, distribution and reproduction in any medium, provided the original work is properly cited.

field structures. Hence, a fundamental question arises: Are solitary DFs the most common magnetic field structures associated with JFs?

Instabilities can develop at the JF and grow to large amplitudes and distort the JF structure leading to more complex DFs (e.g., Balikhin et al., 2014). In particular, perturbations of the JFs can result from the MHD interchange mode (Guzdar et al., 2010; Lapenta & Bettarini, 2011), the kinetic ballooning interchange instability (Pritchett & Coroniti, 2010), the lower-hybrid drift instability (Divin et al., 2015; Pan et al., 2018) and the pressure-anisotropy-driven mirror mode (Zieger et al., 2011) and firehose (Hietala et al., 2015) instabilities. Examples of a solitary DF and a DF with more complex structures are presented in Section 4.2. We use the Magnetospheric Multiscale (MMS) data (Burch et al., 2016) to characterize the magnetic structure of the JFs comparing the occurrence of solitary DFs with respect to DFs with more complex structures.

## 2. Data Sets

We search for BBFs from the five MMS magnetotail seasons: 4 May 2017–30 August 2017, 25 May 2019–28 September 2019, 18 June 2019–5 October 2019, 27 June 2020–9 October 2020, and 26 June 2021–13 October 2021. We use the Fast Survey data. Among all the instruments onboard the MMS spacecraft, we use the magnetic field measurements from the Flux Gate Magnetometer (FGM) (Russell et al., 2016) and the moments of the ion distribution measured by the Fast Plasma Investigation Dual Ion Spectrometer (FPI-DIS) (Pollock et al., 2016). To account for the penetrating radiation, we correct the ion moments using the method described in Gershman et al. (2019). We note that the data is not uniformly distributed over the 5 years, due to the switch off of the FPI instruments during the Earth's shadow encounters, which were longer during the seasons 2019 to 2021. Finally, since the scale of the BBF channel is typically of the order of a few Earth radii (Nakamura et al., 2004) which is much larger than the MMS spacecraft separation of  $\Delta R \sim 10$  km, the spacecraft tetrahedron can be considered as one single spacecraft. Therefore, we use the magnetic field and the ion moments measured by MMS 1 only.

## 3. Spatial Distribution and Duration of BBFs

### 3.1. Selection Criteria

To detect BBFs in the magnetotail, we employ a selection criteria based on the Geocentric Solar Magnetospheric (GSM) Earthward component of the ion bulk velocity  $V_{ix}$ . To allow for comparison with previous studies, we use criteria similar to those used by Baumjohann et al. (1990) and Angelopoulos et al. (1994). The criteria are the following:

1. Peak ion bulk velocity  $|V_{ix}| \geq 300$  km s<sup>-1</sup>.
2. BBF time intervals are defined such that  $|V_{ix}| \geq 100$  km s<sup>-1</sup>.
3. Time records which satisfy condition 1 are clustered with those 60 s apart.
4. Average  $\beta_i > 0.5$  to ensure BBF is in the CPS (Angelopoulos et al., 1994), where  $\beta_i = P_i/P_{mag}$ ,  $P_i$  is the ion plasma pressure, and  $P_{mag} = B^2/2\mu_0$  is the magnetic pressure.
5. To prevent selection of magnetosheath jets (Plaschke et al., 2018), the region of interest is restricted to  $|Y_{GSM}| \leq 12 R_E$ .

We note that our peak velocity threshold is similar to  $|V_{ix}| \geq 300$  km s<sup>-1</sup> used by Ohtani et al. (2004), where  $V_{ix}$  is the Earthward component of the velocity perpendicular to the local magnetic field. This threshold is lower than  $|V_{ix}| \geq 400$  km s<sup>-1</sup> used by Baumjohann et al. (1990) and Angelopoulos et al. (1994), so that the resulting occurrence rate of BBFs may differ from that found in these studies.

### 3.2. Results

We find a total of 2394 BBFs in the CPS, with 2135 Earthward and 259 tailward BBFs. We note that 1796 of the BBFs also satisfy  $\max(|V_{ix}|) \geq 400$  km s<sup>-1</sup> and only 1175 BBFs satisfy  $\max(|V_{ix}|) \geq 500$  km s<sup>-1</sup>. To account for orbital coverage bias, we plot in Figure 1 the projection of the MMS CPS orbital coverage (first row) and the occurrence rate (number of events per bin/orbital hours per bin) of Earthward (second row) and tailward (third row) BBFs. The statistically relevant size of the bin  $h_i$  along the  $i$  GSM axis is estimated using a Freedman-Diaconis estimator  $h_i = 2IQR_i/N^{1/3}$ , where  $IQR_i$  is the interquartile range of the spacecraft position,

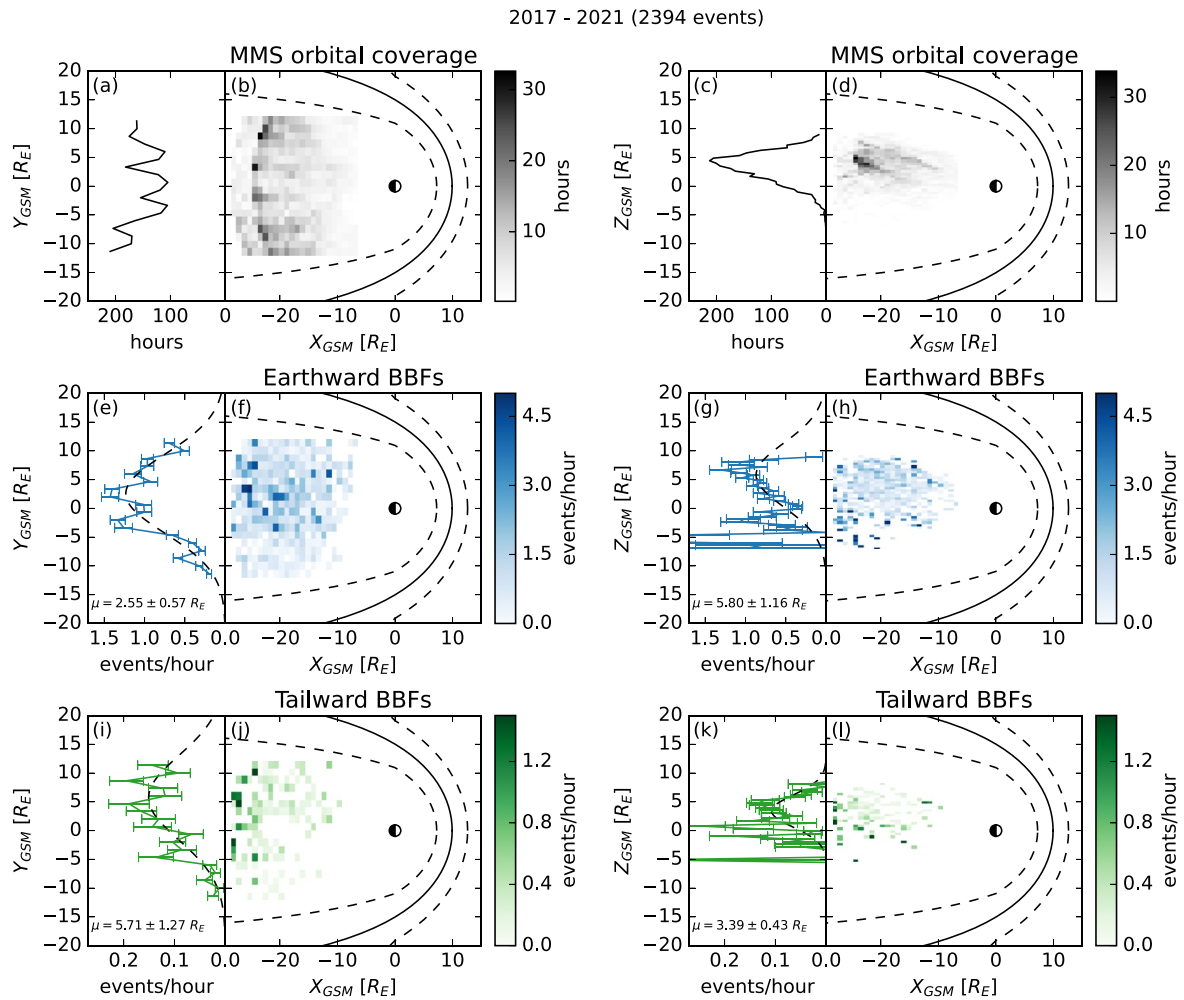


**Figure 1.** Spatial distributions of the Magnetospheric Multiscale (MMS) orbital coverage and Earthward and tailward bursty bulk flows (BBFs). (a) Dawn-dusk, (b) equatorial plane, (c) north-south, and (d) meridional plane projections of the distribution of the MMS orbital coverage. (e) Dawn-dusk, (f) equatorial plane, (g) north-south, and (h) meridional plane projections of the distribution of the occurrence rate of Earthward BBFs. (i) Dawn-dusk, (j) equatorial plane, (k) north-south, and (l) meridional plane projections of the distribution of the occurrence rate of tailward BBFs. The black dashed lines in panels (e, g, i, and k) are the Gaussian fits. The black lines in panels (a, d, f, h, j, and l) are the average (solid line) and  $1\sigma$  boundaries (dashed lines) of the statistical magnetopause from Shue et al. (1998). The error bars are obtained by propagating the standard Poisson statistical uncertainty of each bin count.

and  $N = 2394$  is the total number of BBFs. It yields  $h_x = 0.9 R_E$ ,  $h_y = 1.3 R_E$  and  $h_z = 0.5 R_E$ . Finally, we fit the dawn-dusk (panels e and i) and north-south (panels g and k) projection of the occurrence rate distribution to a Gaussian distribution (black dashed lines) using a Levenberg-Marquardt method of minimization of the  $\chi^2$  cost function.

The MMS CPS orbital coverage is strongly skewed toward the northern GSM hemisphere (Figure 1b), and increases with distance from Earth due to slower orbital velocity near the apogee. The equatorial projection of the orbital coverage (Figure 1a) is not uniformly distributed in magnetic local time (MLT). This somewhat surprising observation is due to rotation of the Earth's magnetic dipole axis which lies in the XZ GSM plane.

The dawn-dusk (Figure 1e) and north-south (Figure 1g) distributions of the Earthward BBFs show clear Gaussian shapes centered at  $\langle Y_{GSM} \rangle = 2.55 \pm 0.57 R_E$  ( $\sigma(Y_{GSM}) = 6.87 \pm 0.59 R_E$ ) and  $Z_{GSM} = 5.80 \pm 1.16 R_E$  ( $\sigma(Z_{GSM}) = 5.55 \pm 1.28 R_E$ ), respectively. The dawn-dusk (Figure 1i) and north-south (Figure 1k) distributions of the tailward BBFs show, similar to that of Earthward BBFs, clear Gaussian shapes centered at  $\langle Y_{GSM} \rangle = 5.71 \pm 1.27 R_E$  ( $\sigma(Y_{GSM}) = 7.34 \pm 0.96 R_E$ ) and  $Z_{GSM} = 3.39 \pm 0.43 R_E$  ( $\sigma(Z_{GSM}) = 2.79 \pm 0.52 R_E$ ), respectively. Since during the MMS magnetotail phase (northern hemisphere summer) the neutral sheet (NS) is statistically located north of

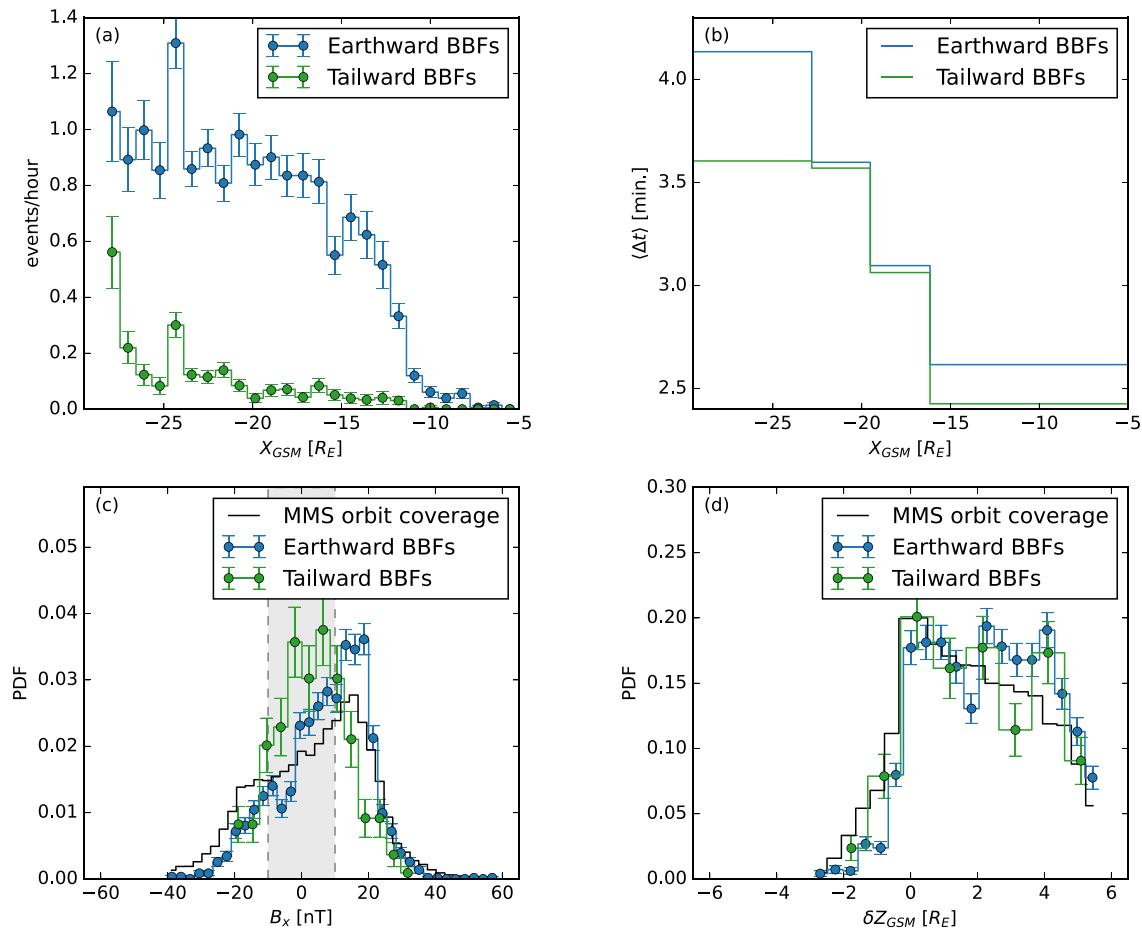


**Figure 2.** Distribution of Earthward (blue) and tailward (green) bursty bulk flows (BBFs) with respect to Earth and NS. (a) Earthward projection of the BBFs occurrence rate. (b) Average duration of the BBFs with respect to distance from Earth. (c) Probability Density Function of  $B_x$  associated with BBFs. The black line indicates the probability density function (PDF) of  $B_z$  measured by Magnetospheric Multiscale (MMS) during all magnetotail seasons. (d) PDF of  $\delta Z_{GSM}$  associated with BBFs. The black line indicates the PDF of  $\delta Z_{GSM}$  computed for MMS during all magnetotail seasons. The error bars are obtained by propagating the standard Poisson statistical uncertainty of each bin count.

the GSM equatorial plane, the northward skewness of the north-south distributions of the Earthward and tailward BBFs is attributed to an observational bias.

Figure 2a shows the occurrence rate of Earthward (blue) and tailward (green) BBFs with respect to  $X_{GSM}$ . The occurrence of Earthward BBFs is constant for  $X_{GSM} \lesssim -19 R_E$ , consistent with the AMPTE/IRM and ISEE 2 statistical study by Angelopoulos et al. (1994), and decreases with distance from Earth in the  $-19 R_E \lesssim X_{GSM} \lesssim -10 R_E$  region. At the same time, the duration of the Earthward and tailward BBFs decreases with distance from Earth (Figure 2b). The occurrence rate of the tailward BBFs is small but non-zero at  $-5 R_E \geq X_{GSM} \gtrsim -15 R_E$ , slightly increases at  $X_{GSM} \sim -21 R_E$ , is constant at  $-21 R_E \gtrsim X_{GSM} \gtrsim -25 R_E$  and rises beyond  $X_{GSM} \lesssim -25 R_E$ .

To estimate the distance from the BBFs to the magnetotail NS, we plot the probability density function (PDF) of  $B_x$ , which is a proxy of the distance to the NS, as well as that of the distance  $\delta Z_{GSM}$  to a model NS (Fairfield, 1980) in Figures 2c and 2d respectively. We also plot the distribution of  $B_x$  and  $\delta Z_{GSM}$  measured during all magnetotail seasons (black). For the Earthward BBFs, the distributions of the two proxies overlaps with that of the background orbital coverage, suggesting that Earthward BBFs can be observed over a large north-south extent. For tailward BBFs, the distribution of  $B_x$  is clearly more centered around the NS ( $|B_x| = 0$  nT) and confined to  $|B_x| < 10$  nT which means that the tailward BBFs are likely to be observed over a narrow north-south extent.

## 4. Occurrence of Dipolarization Fronts Associated With BBFs

### 4.1. Selection Criteria

To characterize the magnetic field structure at JFs, we employ the methods by Schmid et al. (2011) [S11] and Fu et al. (2012) [F12]. The methods are applied to the magnetic field data in 180 s windows. Since the duration of a BBF is given by  $|V_{ix}| > 100 \text{ km s}^{-1}$ , the intervals shorter than 180 s are padded with extra points, while longer intervals are split in 180 s intervals with a 90 s overlap. Since we are interested in the magnetic field structures at the JFs, that is, upstream of the velocity peak, we use only the data before the peak. The following criteria from S11 are then applied to the 180 s windows:

1. Significant change of  $B_z$ :  $|\Delta B_z| = |\max(B_z) - \min(B_z)| \geq 4 \text{ nT}$ .
2. Significant change of inclination angle  $\theta = \arctan \left( B_z / \sqrt{B_x^2 + B_y^2} \right)$ :  $\Delta\theta = \theta(B_z = \max(B_z)) - \theta(B_z = \min(B_z)) \geq 10^\circ$ .
3. Inclination angle close to the dipolar configuration:  $\max(\theta) \geq 45^\circ$ .

These criteria were originally designed to find DFs corresponding to the qualitative picture of DFs as a solitary sharp large-amplitude increase of  $B_z$  (Nakamura et al., 2002; Runov et al., 2009). However, the superposed epoch analysis in S11 shows that the median of the superposed  $B_z$  does not show a distinct sharp increase of  $B_z$  expected for solitary DFs (e.g., Runov et al., 2011). From which we conclude that the S11 criteria corresponds to broader class of large-amplitude changes of  $B_z$  than just the solitary DFs (e.g., plasmoids, more complex DFs, current sheets, etc.). Thus to identify the solitary DFs, we in addition employ the F12 method, which relies on fitting the  $B_z$  increase by a hyperbolic tangent function:

$$B_{fit} = \frac{a}{2} \tanh \left( \frac{t - t_{DF}}{b/2} \right) + \left( c + \frac{a}{2} \right), \quad (1)$$

where  $t_{DF}$  is the time of the candidate DF. First, we determine  $t_{DF}$  as the time of maximum of the time derivative of  $B_z$  smoothed using a fifth order Savitzky–Golay filter on a time scale of  $0.5 f_{ci}^{-1}$ . This is different from that done in F12 who used  $t_{DF} = (t_{\min(B_z)} + t_{\max(B_z)}) / 2$ . Then, we fit  $B_z$  in the interval  $[t_{DF} - 30 \text{ s}, t_{DF} + 15 \text{ s}]$ . Finally, we employ criteria on the amplitude  $|a| \geq 4 \text{ nT}$ , the time scale  $b \leq 8 \text{ s}$  and the root-mean square residual  $\sigma = \sqrt{\langle |B_z - B_{fit}|^2 \rangle} \leq |a|/2$ . In contrast to the constant  $\sigma \leq 2.5 \text{ nT}$  used in F12, we use a criteria which depends on the amplitude of the  $B_z$  jump. This modified criteria results in reliable DF detection even in the presence of a  $B_z$  dip ahead of the DF or a fast decrease of  $B_z$  behind the front.

### 4.2. Results

The left column of Figure 3 shows an example of a BBF front with a solitary DF, that is, that satisfies both S11 and F12-based criteria. We observe that the time of the DF  $t_{DF}$  (orange dashed line) matches the ion energy enhancement (panel a), the ion density  $n_i$  decrease (panel c) and the ion temperature  $T_i$  increase (panel e), which indicates that our method provides an accurate estimate of  $t_{DF}$ . This case presents a solitary large-amplitude sharp increase of  $B_z$  and thus corresponds to the qualitative picture of a solitary DF. The fitting procedure applied to  $B_z$  (panel f) yields the amplitude  $a = 6.7 \text{ nT}$ , the time scale  $b = 0.97 \text{ s}$  and the residual  $\sigma = 1.19 \text{ nT}$  that satisfy the F12-based criteria, so this JF is classified as a solitary DF.

The right column of Figure 3 presents an example of a BBF front which satisfies the S11 criteria but not the F12-based criteria. This event was first reported by Alqeeq et al. (2022) to show the non-homogeneity of the energy conversion due to electron-scale substructures attributed to lower-hybrid drift waves. Similar to the other example,  $t_{DF}$  is accurately estimated as it corresponds to the ion energy enhancement (panel g), the ion density  $n_i$  decrease (panel i) and the ion temperature  $T_i$  increase (panel k). This JF is associated with multiple ion-scale magnetic field structures (panel h). Thus, this JF is not a solitary DF but it corresponds to a broader class of more complex DFs. As a result, the F12 fitting procedure applied to the  $B_z$  component of the complex magnetic field structures (panel l) yields parameters which do not satisfy the F12-based criteria. So this JF example, which satisfies the S11 criteria but not the F12-based criteria, is not classified as a solitary DF but as a DF with more complex structures.

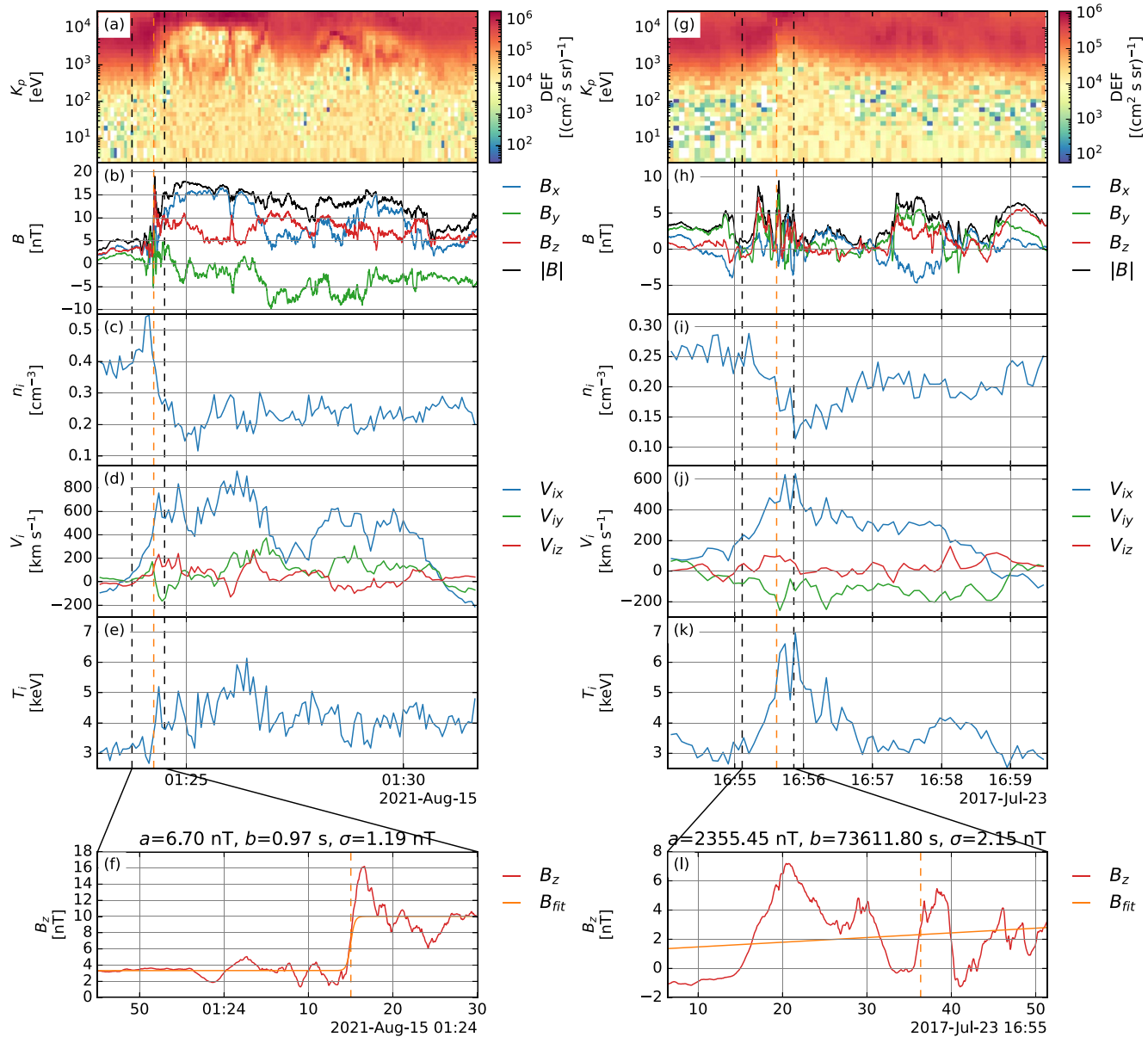


**Figure 3.** Examples of a “classical” solitary dipolarization front (DF) (left) and “turbulent” jet front (JF) (right). (a and g) Ion differential energy flux spectrum. (b and h) Magnetic field in Geocentric Solar Magnetospheric (GSM) coordinates. (c and i) Ion number density. (d and j) Ion bulk velocity in GSM coordinates. (e and k) Ion temperature. (f and l)  $B_z$  used for fitting (red) and fitted magnetic field (orange). The orange dashed lines indicate the estimated times of the candidates dipolarization fronts (see text).

**Table 1**  
Occurrence of Quiet, Dipolarization Front Associated and “Turbulent”  
Bursty Bulk Flows (BBFs)

Criteria	Earthward BBFs	Tailward BBFs	All BBFs
Quiet JFs S11	1231 (58%)	150 (58%)	1381 (58%)
Solitary DFs S11 $\cap$ F12	238 (11%)	9 (3%)	247 (10%)
“Turbulent” JFs S11 – F12	666 (31%)	100 (39%)	766 (32%)
Total	2135 (100%)	259 (100%)	2394 (100%)

We obtain a total of 1013 BBFs which satisfy the S11 criteria, with 904 Earthward BBFs and 109 tailward BBFs. Among the 1013 BBFs that satisfy S11 criteria, we find that only 247 also satisfy F12-based criteria with 238 Earthward BBFs and 9 tailward BBFs. Since JFs that satisfy the S11 but not F12-based criteria are associated with magnetic field structures more complex than solitary DFs, we refer to them as “turbulent” JFs. There are in total 766 of such BBFs. The remaining 1381 of the BBFs do not satisfy S11 criteria. These BBFs have relatively small changes of  $B_z$  so we refer to them as quiet JFs. We summarize the occurrence of each type of JFs (quiet, solitary DF, and “turbulent” JFs) in Table 1. The percentages are given in terms of total number of Earthward, tailward and all BBFs. About half (42%) of the

JFs are associated with significant increase in  $B_z$ ,  $|\Delta B_z| > 4$  nT. Among these events, “turbulent” JFs are 3 times more common than JFs with a solitary DF.

## 5. Discussion

Using the MMS observations, we found 2394 BBFs in the CPS. We find that the distribution of both Earthward and tailward BBFs is skewed toward the dusk side. Similar dawn-dusk asymmetry was observed by McPherron et al. (2011) using THEMIS, who showed that Earthwards BBFs are predominantly found in the pre-midnight sector. Lu et al. (2016) suggested that the dawn-dusk asymmetry of the magnetotail results from a stronger Hall electric field on the dusk side which is due to higher perpendicular ion temperature, thinner current sheet and small  $B_z$ . We find that the occurrence rate of the Earthward BBFs decreases with distance to Earth, suggesting that Earthward BBFs are decelerated in their course to the Earth leading to a threshold effect in the selection of BBFs. The deceleration of the BBFs during their Earthward convection has been attributed to deflection due to diamagnetic drift which results from magnetic pressure increase (Angelopoulos et al., 1993), the Joule dissipation (Zhang et al., 2020), or energy loss through emission of kinetic Alfvén waves (Angelopoulos et al., 2002; Chaston et al., 2012). We showed that the duration of the Earthward BBFs decreases with distance to Earth, which can be due to our choice of  $|V_{ix}| > 100$  km s<sup>−1</sup> wide intervals, so that slower BBFs are artificially shortened.

At distances where the Earthward BBFs decelerate, we showed a small but non-zero occurrence of tailward BBFs. Tailward BBFs at distances  $-5 R_E \geq X_{GSM} \gtrsim -15 R_E$  can result from velocity shear/magnetic field line twist induced eddies at the edges of the Earthward flow channel (Birn et al., 2004; Keiling et al., 2009; Zhang et al., 2019), kinetic ballooning interchange instability (Pritchett & Coroniti, 2010), or flow rebounds (Chen & Wolf, 1999; Ohtani et al., 2009; Panov et al., 2010). The latter mechanism was suggested by Ohtani et al. (2009), to be the most likely cause of tailward BBFs, which are often preceded with Earthward BBFs. However, here, we found that only 18 (1.7%) tailward BBFs in the  $-5 R_E \geq X_{GSM} \gtrsim -20 R_E$  are preceded (within 10 min) by an Earthward BBF. This result suggests that the incident Earthward convected flux tube is non-specularly reflected from its equilibrium (Ohtani et al., 2009), or that the tailward BBFs are much slower than the incident Earthward BBFs resulting from heavy damping of the oscillations of the flux tube (Chen & Wolf, 1999; Panov et al., 2010).

Using the  $B_z$  fitting based on the method by Fu et al. (2012), we find that only 10% of the BBFs fronts contain a solitary DF at their front. This result contradicts the superposed Epoch analysis carried out by Ohtani et al. (2004) and Wiltberger et al. (2015) using Geotail observations and the Lyon-Fedder-Mobarry global MHD magnetosphere model. Ohtani et al. (2004) and Wiltberger et al. (2015) showed that the magnetic field convected Earthward with the fast flows has a dipolar configuration at the JF. However, in their analysis Ohtani et al. (2004) and Wiltberger et al. (2015) selected the BBFs based on ion velocity  $V_{ix}$  perpendicular to the local magnetic field, which implicitly constrains the magnetic field to a dipolar configuration (large  $B_z$ ), and therefore restrict the events to JFs with a solitary DF. Our results suggest that the “classical” picture of a solitary DF (e.g., Runov et al., 2011) is not the most likely magnetic field structure associated with the JF.

Furthermore, using the selection criteria proposed by Schmid et al. (2011) to detect magnetic field changes, we show that these criteria allow us to detect not only the solitary DFs but also more complex structures at the JF. In particular, we found that 32% of the BBFs are associated with complex structures other than a solitary DF. The abundance of such complex structures at the JF over solitary DF can be explained by the wide variety of instabilities which can develop at fronts of BBFs, such as the MHD interchange instability (Guzdar et al., 2010; Lapenta & Bettarini, 2011), the kinetic ballooning interchange instability (Pritchett & Coroniti, 2010), the lower-hybrid drift instability (Divin et al., 2015) and the pressure-anisotropy-driven mirror mode (Zieger et al., 2011) and firehose (Hietala et al., 2015) instabilities. The growth of the aforementioned instabilities results in electromagnetic fluctuations modifying the JF structure. These fluctuations in turn dissipate into particle energy through plasma heating (Angelopoulos et al., 2013; Khotyaintsev et al., 2017) and particle acceleration (Greco et al., 2017; Khotyaintsev et al., 2011). The energy cascade of the free energy injected at the jet scale to the kinetic scales, suggests that turbulence develops within the BBFs (Bandyopadhyay et al., 2020; Huang et al., 2012; Pucci et al., 2017; Vörös et al., 2006). Our results suggest that BBFs accompanied with “turbulent” JF with magnetic field oscillations are 3 times more likely than BBFs associated with a solitary DF.

## 6. Conclusion

We compiled a database of 2394 plasma sheet jets (BBFs), which show statistical properties similar to the ones known from earlier studies (Angelopoulos et al., 1994; Baumjohann et al., 1990; McPherron et al., 2011). We characterize the structure of the JFs using the criteria by Schmid et al. (2011) and the method introduced by Fu et al. (2012) with a new technique based on the magnetic field gradient to estimate the time of the candidate DF. We find that only 10% of the JFs are associated solitary sharp and strong dipolarization of the magnetic field corresponding to the qualitative description of a solitary DF (e.g., Runov et al., 2011). About half (42%) of JFs are associated with large variations of the north-south component of the magnetic field  $B_z$ ,  $|\Delta B_z| > 4$  nT. Solitary DFs, constitute a quarter of these events, while the rest are associated with more complicated magnetic field structures that is, “turbulent.” Our results indicate that the “classical” picture of a solitary DF as the magnetic field structure associated with the JF is not the most commonly occurring magnetic field structure, which points at instabilities to drive ion to electron-scale perturbations modifying the structure of the magnetotail plasma JFs (Balikhin et al., 2014).

## Data Availability Statement

Magnetospheric multiscale data are available at <https://lasp.colorado.edu/mms/sdc/public/data/> following the directories: mms1/fgm/srvy/l2 for Flux Gate Magnetometer (FGM) data, mms1/fpi/fast/l2/dis-moms for FPI ion moments. Data analysis was performed using the pyrfu analysis package. The codes to reproduce the figures in this paper are available at <https://github.com/louis-richard/bbfstats>. The compiled bursty bulk flows (BBFs) database and additional data are available at <https://doi.org/10.5281/zenodo.7009706>.

## Acknowledgments

We thank the entire Magnetospheric Multiscale team and instrument PIs for data access and support. LR thanks A. Lalti, C. Norgren, and the International Space Science Institute working group on “Magnetotail Dipolarizations: Archimedes Force or Ideal Collapse?” for valuable discussions. This work is supported by the Swedish National Space Agency Grant 139/18.

## References

- Alqeeq, S. W., Le Contel, O., Canu, P., Retinò, A., Chust, T., Mirioni, L., et al. (2022). Investigation of the homogeneity of energy conversion processes at dipolarization fronts from MMS measurements. *Physics of Plasmas*, 29(1), 012906. <https://doi.org/10.1063/5.0069432>
- Angelopoulos, V., Chapman, J. A., Mozer, F. S., Scudder, J. D., Russell, C. T., Tsuruda, K., et al. (2002). Plasma sheet electromagnetic power generation and its dissipation along auroral field lines. *Journal of Geophysical Research*, 107(A8), A81181. <https://doi.org/10.1029/2001JA900136>
- Angelopoulos, V., Kennel, C. F., Coroniti, F. V., Pellat, R., Kivelson, M. G., Walker, R. J., et al. (1994). Statistical characteristics of bursty bulk flow events. *Journal of Geophysical Research*, 99(A11), 21257–21280. <https://doi.org/10.1029/94JA01263>
- Angelopoulos, V., Kennel, C. F., Coroniti, F. V., Pellat, R., Spence, H. E., Kivelson, M. G., et al. (1993). Characteristics of ion flow in the quiet state of the inner plasma sheet. *Geophysical Research Letters*, 20(16), 4–1714. <https://doi.org/10.1029/93GL00847>
- Angelopoulos, V., Runov, A., Zhou, X.-Z., Turner, D. L., Kiehas, S. A., Li, S.-S., & Shinora, S. (2013). Electromagnetic energy conversion at reconnection fronts. *Science*, 341(6153), 1478–1482. <https://doi.org/10.1126/science.1236992>
- Artemyev, A. V., Lutsenko, V. N., & Petrukovich, A. A. (2012). Ion resonance acceleration by dipolarization fronts: Analytic theory and spacecraft observation. *Annales Geophysicae*, 30(2), 317–324. <https://doi.org/10.5194/angeo-30-317-2012>
- Balikhin, M. A., Runov, A., Walker, S. N., Gedalin, M., Dandouras, I., Hobara, Y., & Fazakerley, A. (2014). On the fine structure of dipolarization fronts. *Journal of Geophysical Research: Space Physics*, 119(8), 6367–6385. <https://doi.org/10.1002/2014JA019908>
- Bandyopadhyay, R., Chasapis, A., Gershman, D. J., Giles, B. L., Russell, C. T., Strangeway, R. J., et al. (2020). Observation of an inertial-range energy cascade within a reconnection jet in the Earth’s magnetotail. *Monthly Notices of the Royal Astronomical Society: Letters*, 500(1), L6–L10. <https://doi.org/10.1093/mnrasl/laaa171>
- Baumjohann, W., Paschmann, G., & Lühr, H. (1990). Characteristics of high-speed ion flows in the plasma sheet. *Journal of Geophysical Research*, 95(A4), 3801. <https://doi.org/10.1029/JA095iA04p03801>
- Birn, J., Raeder, J., Wang, Y. L., Wolf, R. A., & Hesse, M. (2004). On the propagation of bubbles in the geomagnetic tail. *Annales Geophysicae*, 22(5), 1773–1786. <https://doi.org/10.5194/angeo-22-1773-2004>
- Burch, J. L., Moore, T. E., Torbert, R. B., & Giles, B. L. (2016). Magnetospheric multiscale overview and science objectives. *Space Science Reviews*, 199(1–4), 5–21. <https://doi.org/10.1007/s11214-015-0164-9>
- Chaston, C. C., Bonnell, J. W., Clausen, L., & Angelopoulos, V. (2012). Correction to “Energy transport by kinetic-scale electromagnetic waves in fast plasma sheet flows”. *Journal of Geophysical Research*, 117(A12). <https://doi.org/10.1029/2012JA018476>
- Chen, C. X., & Wolf, R. A. (1999). Theory of thin-filament motion in Earth’s magnetotail and its application to bursty bulk flows. *Journal of Geophysical Research*, 104(A7), 14613–14626. <https://doi.org/10.1029/1999JA900005>
- Divin, A., Khotyaintsev, Y. V., Vaivads, A., & André, M. (2015). Lower hybrid drift instability at a dipolarization front. *Journal of Geophysical Research: Space Physics*, 120(2), 1124–1132. <https://doi.org/10.1002/2014JA020528>
- Fairfield, D. (1980). A statistical determination of the shape and position of the geomagnetic neutral sheet. *Journal of Geophysical Research*, 85(A2), 775–780. <https://doi.org/10.1029/JA085iA02p00775>
- Fu, H. S., Khotyaintsev, Y. V., André, M., & Vaivads, A. (2011). Fermi and betatron acceleration of suprathermal electrons behind dipolarization fronts. *Geophysical Research Letters*, 38(16), L16104. <https://doi.org/10.1029/2011GL048528>
- Fu, H. S., Khotyaintsev, Y. V., Vaivads, A., André, M., & Huang, S. Y. (2012). Occurrence rate of earthward-propagating dipolarization fronts. *Geophysical Research Letters*, 39(10). <https://doi.org/10.1029/2012GL051784>
- Gershman, D. J., Dorelli, J. C., Avakov, L. A., Gliese, U., Barrie, A., Schiff, C., et al. (2019). Systematic uncertainties in plasma parameters reported by the Fast Plasma Investigation on NASA’s Magnetospheric Multiscale mission. *Journal of Geophysical Research: Space Physics*, 124(12), 10345–10359. <https://doi.org/10.1029/2019JA026980>

- Greco, A., Artemyev, A., Zimbardo, G., Angelopoulos, V., & Runov, A. (2017). Role of lower hybrid waves in ion heating at dipolarization fronts. *Journal of Geophysical Research: Space Physics*, 122(5), 5092–5104. <https://doi.org/10.1002/2017JA023926>
- Guzdar, P. N., Hassam, A. B., Swisdak, M., & Sitnov, M. I. (2010). A simple MHD model for the formation of multiple dipolarization fronts. *Geophysical Research Letters*, 37(20). <https://doi.org/10.1029/2010GL045017>
- Hietala, H., Drake, J. F., Phan, T. D., Eastwood, J. P., & McFadden, J. P. (2015). Ion temperature anisotropy across a magnetotail reconnection jet. *Geophysical Research Letters*, 42(18), 7239–7247. <https://doi.org/10.1002/2015GL065168>
- Huang, S. Y., Zhou, M., Sahraoui, F., Vaivads, A., Deng, X. H., André, M., et al. (2012). Observations of turbulence within reconnection jet in the presence of guide field. *Geophysical Research Letters*, 39(11). <https://doi.org/10.1029/2012GL052210>
- Keiling, A., Angelopoulos, V., Runov, A., Weygand, J., Apatenkov, S. V., Mende, S., et al. (2009). Substorm current wedge driven by plasma flow vortices: THEMIS observations. *Journal of Geophysical Research*, 114(A1). <https://doi.org/10.1029/2009JA014114>
- Khotyaintsev, Y. V., Cully, C. M., Vaivads, A., André, M., & Owen, C. J. (2011). Plasma jet braking: Energy dissipation and nonadiabatic electrons. *Physical Review Letters*, 106(16), 165001. <https://doi.org/10.1103/PhysRevLett.106.165001>
- Khotyaintsev, Y. V., Divin, A., Vaivads, A., André, M., & Markidis, S. (2017). Energy conversion at dipolarization fronts. *Geophysical Research Letters*, 44(3), 1234–1242. <https://doi.org/10.1002/2016GL071909>
- Lapenta, G., & Bettarini, L. (2011). Self-consistent seeding of the interchange instability in dipolarization fronts. *Geophysical Research Letters*, 38(11). <https://doi.org/10.1029/2011GL047742>
- Liu, J., Angelopoulos, V., Zhou, X.-Z., Yao, Z.-H., & Runov, A. (2015). Cross-tail expansion of dipolarizing flux bundles. *Journal of Geophysical Research: Space Physics*, 120(4), 2516–2530. <https://doi.org/10.1002/2015JA020997>
- Lu, S., Lin, Y., Angelopoulos, V., Artemyev, A. V., Pritchett, P. L., Lu, Q., & Wang, X. Y. (2016). Hall effect control of magnetotail dawn-dusk asymmetry: A three-dimensional global hybrid simulation: Hall magnetotail dawn-dusk asymmetry. *Journal of Geophysical Research: Space Physics*, 121(12), 11882–11895. <https://doi.org/10.1002/2016JA023325>
- McPherron, R. L., Hsu, T.-S., Kissinger, J., Chu, X., & Angelopoulos, V. (2011). Characteristics of plasma flows at the inner edge of the plasma sheet. *Journal of Geophysical Research*, 116(A5). <https://doi.org/10.1029/2010JA015923>
- Nakamura, R., Baumjohann, W., Klecker, B., Bogdanova, Y., Balogh, A., Rème, H., et al. (2002). Motion of the dipolarization front during a flow burst event observed by Cluster. *Geophysical Research Letters*, 29(20), 1942–3–4. <https://doi.org/10.1029/2002GL015763>
- Nakamura, R., Baumjohann, W., Mouikis, C., Kistler, L. M., Runov, A., Volwerk, M., et al. (2004). Spatial scale of high-speed flows in the plasma sheet observed by Cluster. *Geophysical Research Letters*, 31(9), L09804. <https://doi.org/10.1029/2004GL019558>
- Ohtani, S., Miyashita, Y., Singer, H., & Mukai, T. (2009). Tailward flows with positive BZ in the near-Earth plasma sheet. *Journal of Geophysical Research*, 114(A6), A06218. <https://doi.org/10.1029/2009JA014159>
- Ohtani, S., Shay, M. A., & Mukai, T. (2004). Temporal structure of the fast convective flow in the plasma sheet: Comparison between observations and two-fluid simulations. *Journal of Geophysical Research*, 109(A3), A03210. <https://doi.org/10.1029/2003JA010002>
- Pan, D., Khotyaintsev, Y. V., Graham, D. B., Vaivads, A., Zhou, X., André, M., et al. (2018). Rippled electron-scale structure of a dipolarization front. *Geophysical Research Letters*, 45(22), 12116–12124. <https://doi.org/10.1029/2018GL080826>
- Panov, E. V., Nakamura, R., Baumjohann, W., Angelopoulos, V., Petrukovich, A. A., Retinò, A., et al. (2010). Multiple overshoot and rebound of a bursty bulk flow. *Geophysical Research Letters*, 37(8). <https://doi.org/10.1029/2009GL041971>
- Plaschke, F., Hietala, H., Archer, M., Blanco-Cano, X., Kajdič, P., Karlsson, T., et al. (2018). Jets downstream of collisionless shocks. *Space Science Reviews*, 214(5), 81. <https://doi.org/10.1007/s11214-018-0516-3>
- Pollock, C., Moore, T., Jacques, A., Burch, J., Gliese, U., Saito, Y., et al. (2016). Fast plasma investigation for magnetospheric multiscale. *Space Science Reviews*, 199(1–4), 331–406. <https://doi.org/10.1007/s11214-016-0245-4>
- Pritchett, P. L., & Coroniti, F. V. (2010). A kinetic ballooning/interchange instability in the magnetotail. *Journal of Geophysical Research*, 115(A06301). <https://doi.org/10.1029/2009JA014752>
- Pucci, F., Servidio, S., Sorriso-Valvo, L., Olshevsky, V., Matthaeus, W. H., Malara, F., et al. (2017). Properties of turbulence in the reconnection exhaust: Numerical simulations compared with observations. *The Astrophysical Journal*, 841(1), 60. <https://doi.org/10.3847/1538-4357/aa704f>
- Runov, A., Angelopoulos, V., Sitnov, M. I., Sergeev, V. A., Bonnell, J., McFadden, J. P., et al. (2009). THEMIS observations of an earthward-propagating dipolarization front. *Geophysical Research Letters*, 36(14), L14106. <https://doi.org/10.1029/2009GL038980>
- Runov, A., Angelopoulos, V., Zhou, X.-Z., Zhang, X.-J., Li, S., Plaschke, F., & Bonnell, J. (2011). A THEMIS multicasestudy of dipolarization fronts in the magnetotail plasma sheet. *Journal of Geophysical Research*, 116(A5), A05216. <https://doi.org/10.1029/2010JA016316>
- Russell, C. T., Anderson, B. J., Baumjohann, W., Bromund, K. R., Dearborn, D., Fischer, D., et al. (2016). The magnetospheric multiscale magnetometers. *Space Science Reviews*, 199(1–4), 189–256. <https://doi.org/10.1007/s11214-014-0057-3>
- Schmid, D., Volwerk, M., Nakamura, R., Baumjohann, W., & Heyn, M. (2011). A statistical and event study of magnetotail dipolarization fronts. *Annales Geophysicae*, 29(9), 1537–1547. <https://doi.org/10.5194/angeo-29-1537-2011>
- Schmid, D., Volwerk, M., Plaschke, F., Nakamura, R., Baumjohann, W., Wang, G., et al. (2019). Dipolarization fronts: Tangential discontinuities? On the spatial range of validity of the MHD jump conditions. *Journal of Geophysical Research: Space Physics*, 124(12), 9963–9975. <https://doi.org/10.1029/2019JA027189>
- Sergeev, V. A., Angelopoulos, V., Gosling, J. T., Cattell, C. A., & Russell, C. T. (1996). Detection of localized, plasma-depleted flux tubes or bubbles in the midtail plasma sheet. *Journal of Geophysical Research*, 101(A5), 10817–10826. <https://doi.org/10.1029/96JA00460>
- Shue, J.-H., Song, P., Russell, C. T., Steinberg, J. T., Chao, J. K., Zastenker, G., et al. (1998). Magnetopause location under extreme solar wind conditions. *Journal of Geophysical Research*, 103(A8), 17691–17700. <https://doi.org/10.1029/98JA01103>
- Sitnov, M. I., Swisdak, M., & Divin, A. V. (2009). Dipolarization fronts as a signature of transient reconnection in the magnetotail. *Journal of Geophysical Research*, 114(A04202). <https://doi.org/10.1029/2008JA013980>
- Vörös, Z., Baumjohann, W., Nakamura, R., Volwerk, M., & Runov, A. (2006). Bursty bulk flow driven turbulence in the Earth's plasma sheet. *Space Science Reviews*, 122(1–4), 301–311. <https://doi.org/10.1007/s11214-006-6987-7>
- Wiltberger, M., Merkin, V., Lyon, J. G., & Ohtani, S. (2015). High-resolution global magnetohydrodynamic simulation of bursty bulk flows. *Journal of Geophysical Research: Space Physics*, 120(6), 4555–4566. <https://doi.org/10.1002/2015JA021080>
- Zhang, L. Q., Baumjohann, W., Dai, L., Khotyaintsev, Y. V., & Wang, C. (2019). Measurements of the vorticity in the bursty bulk flows. *Geophysical Research Letters*, 46(17–18), 10322–10329. <https://doi.org/10.1029/2019GL084597>
- Zhang, L. Q., Baumjohann, W., Khotyaintsev, Y. V., Burch, J. L., Webster, J., Wang, J. Y., et al. (2020). BBF deceleration down-tail of X < -15 R<sub>E</sub> from MMS observation. *Journal of Geophysical Research: Space Physics*, 125(2). <https://doi.org/10.1029/2019JA026837>
- Zieger, B., Retinò, A., Nakamura, R., Baumjohann, W., Vaivads, A., & Khotyaintsev, Y. (2011). Jet front-driven mirror modes and shocklets in the near-Earth flow-braking region. *Geophysical Research Letters*, 38(22). <https://doi.org/10.1029/2011GL049746>